Electronic Supplementary Material (ESI) for Nanoscale.

Supplementary Information to Tunable High Aspect Ratio Polymer Nanostructures for Cell Interfaces

Kai Sandvold Beckwith,* Simon P. Cooil, Justin W. Wells, and Pawel Sikorski

Department of Physics, Norwegian University of Science and Technology, Trondheim, Norway

E-mail: kai.beckwith@ntnu.no

Table 1: Optimal electron beam exposure doses ensuring high aspect ratio nanostructures using single-pixel dot or single-pixel line exposures in 1 µm SU-8 resist on glass. These doses are above the absolute minimum for standing features, to ensure 100% yield. For thinner SU-8 films (possible down to 100 nm) the same doses can be used successfully to achieve ~ 100 nm features, although lower doses should be used to reach the smallest feature size possible.

Spacing	Pillar dose [aC]	Line dose [pC cm^{-1}]
0.75 µm	2250	N/A
1 µm	2400	50
2 µm	2600	60
5 µm	2750	70
10 µm	2750	70

*To whom correspondence should be addressed

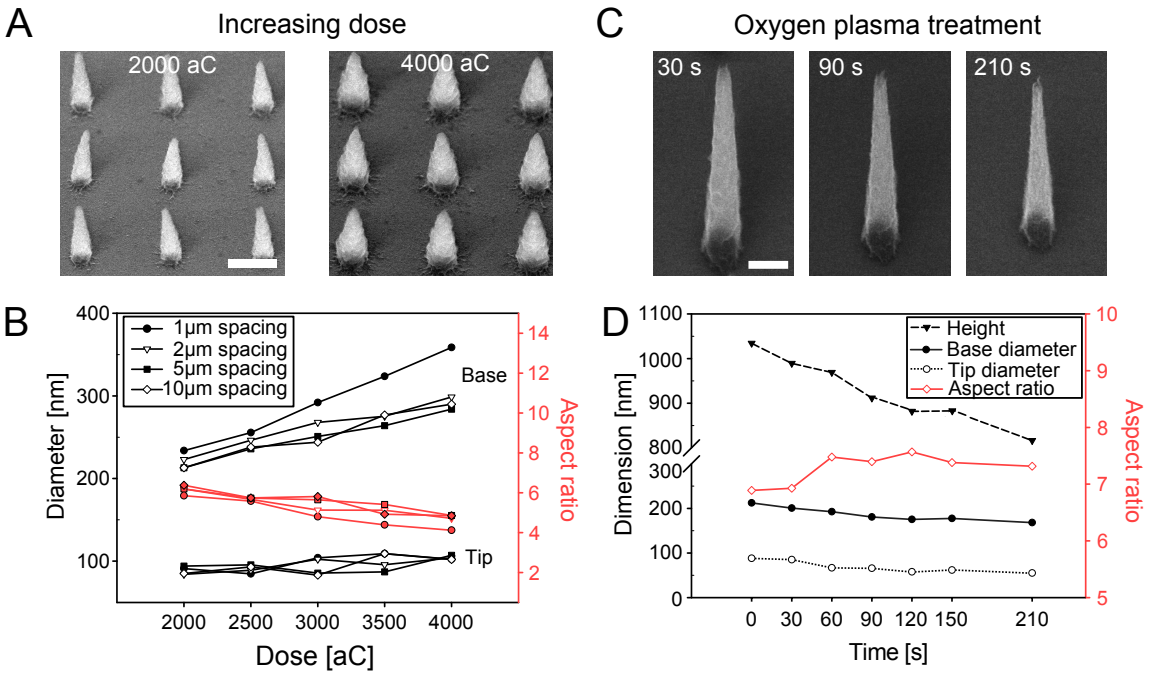

Figure S 1: (A) Tilted SEM images of 1 µm high nanopillars with a 1 µm spacing, with exposure doses of 2000 aC and 4000 aC, showing feature broadening with increasing dose. Scale bar 500 nm. (B) Base and tip diameters (defined as the cross-section 100 nm from the respective apexes) of 1 µm SU-8 nanopillars at various inter-pillar spacings and exposure doses were measured. The associated aspect ratios, defined as the height of the nanopillars divided by the average of the base and tip diameters was also calculated. In particular, nanopillars with 1 µm spacing show increased base broadening at higher doses compared to e.g. nanopillars with ≥ 2 µm spacing, while the tip diameter does not increase as much. (C) Nanopillars were etched by increasing exposure times to oxygen plasma, which reduced both diameter and height of the nanopillars. Scale bar 200 nm. (D) Measured base diameter, tip diameter and height of nanopillars exposed to oxygen plasma for 0-120 s.

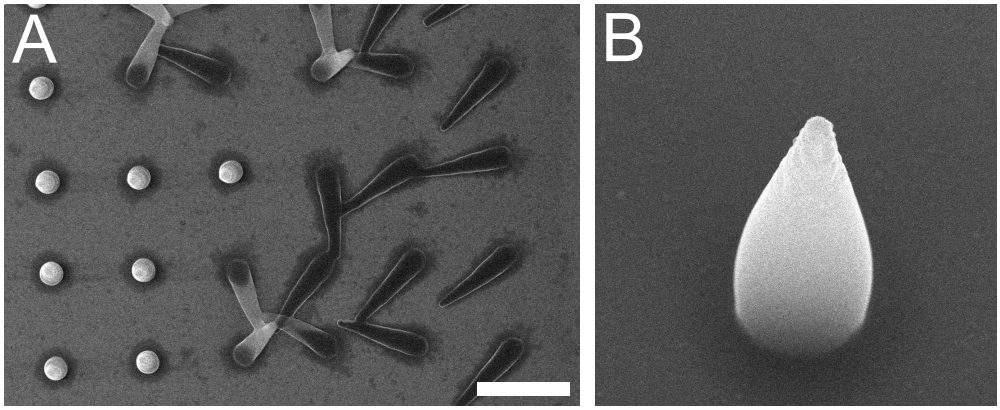

Figure S 2: Possibly encountered issues during processing. (A) Due to under-exposure, some pillars have collapsed during development due to capillary forces. To avoid this, increase dose or increase PEB time. (B) If thick resist films are used (2 µm is shown here), electron scattering through the resist causes features to become increasingly drop-shaped and broad towards the base. The maximum SU-8 thickness that gives relatively straight side-walls on the nanostructures depends on the acceleration voltage of the EBL system, but was around 1 µm for our 30 kV system.

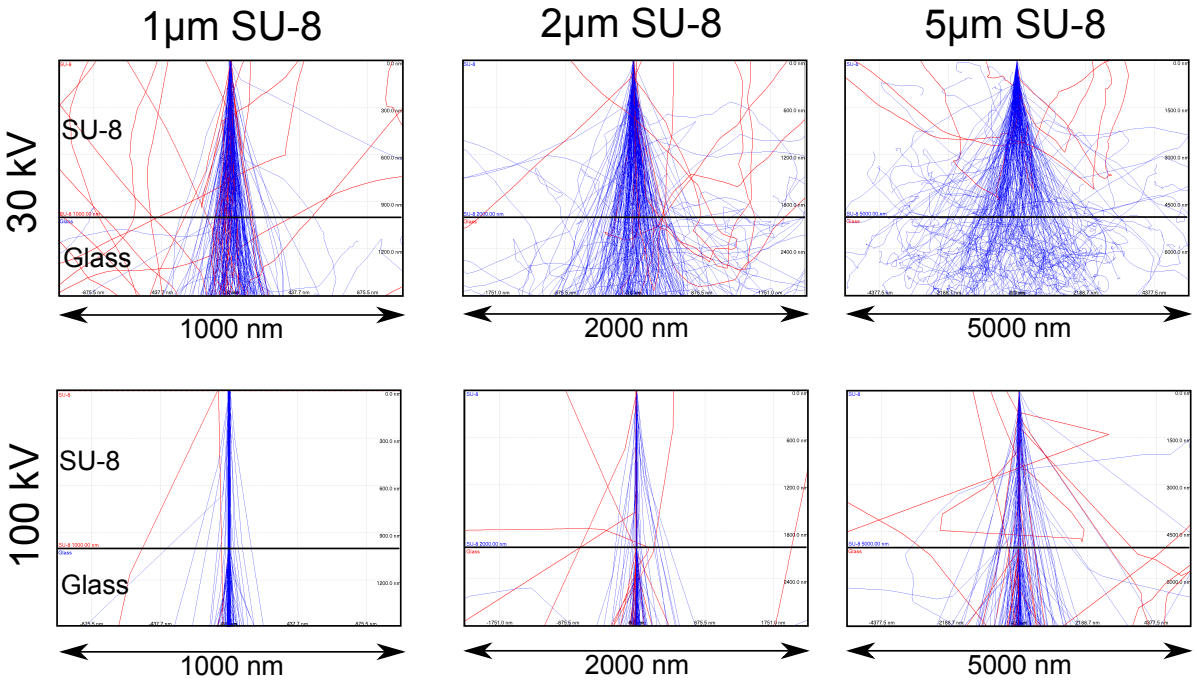

Figure S 3: Simulations of electron trajectories through SU-8 films of 1, 2 and 5 µm thickness on glass substrates with acceleration voltages of 30 and 100 kV. Blue trajectories are forward scattered electrons, while red trajectories are backscattered electrons, secondary electrons are not shown. Thicker resist films give more electron scattering, broadening features and reducing the minimal feature spacing possible. However, these effects are greatly diminished at 100 kV compared to 30 kV, indicating possibilities to make higher aspect ration nanostructures with 100 kV electron beam lithography systems. Simulations performed in Wincasino v. 2.48.

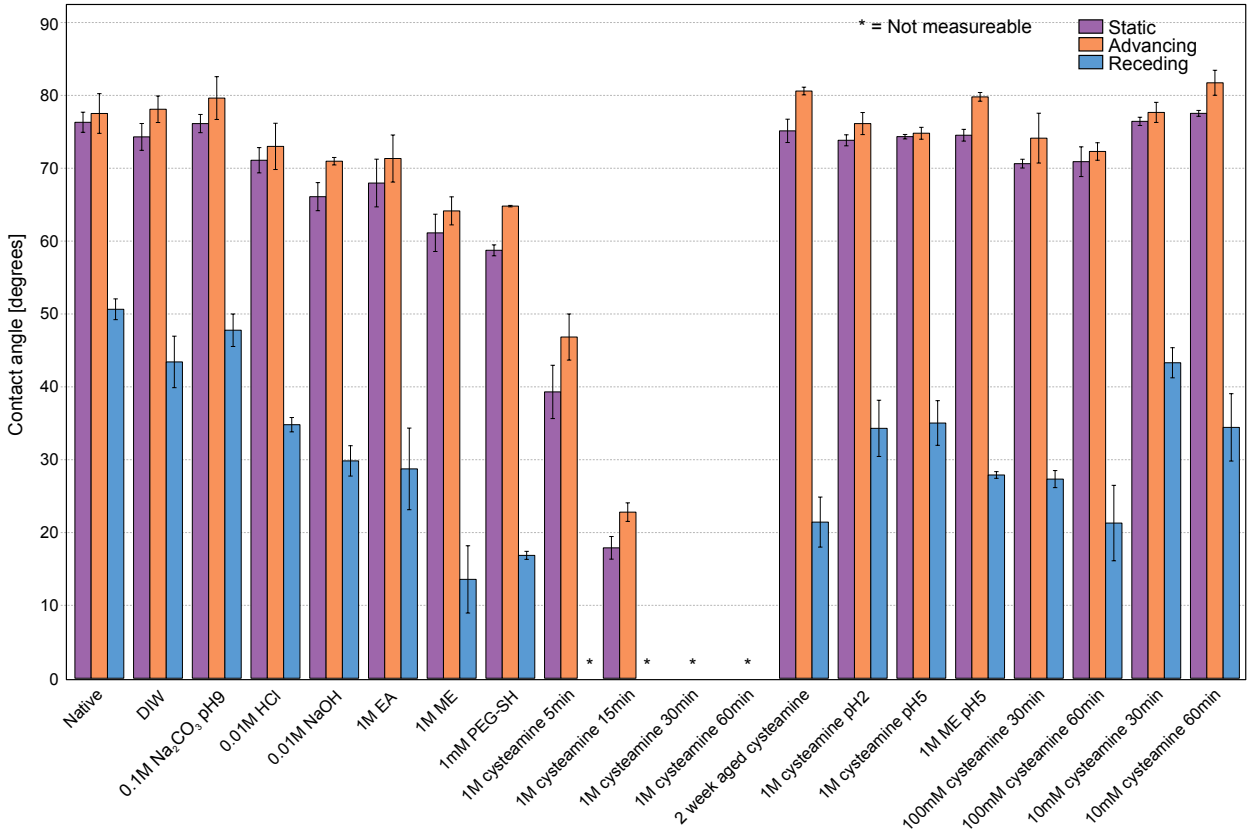

Figure S 4: Static, advancing and receding contact angles after SU-8 surface modifications. Treatment time was 60 minutes unless otherwise indicated, and performed at room temperature. EA = ethanolamine, ME=β-mercaptoethanol. If the contact angle was below approximately 10° it was deemed too low to measure and denoted by *. Most treatments except those with thiolates at pH 8-9 made only small changes in the contact angles. Thiolates at lower pH, aged working solutions (due to autooxidation) as well as lower concentrations showed reduced or absent alteration of contact angles, indicating a low reactivity.

Notes on surface contamination of glass after SU-8 processing

During initial experiments on fluorescent labelling of modified SU-8 with NHS-rhodamine, a significant background signal was observed on the glass surrounding the measured SU-8 features, especially on cysteamine-modified samples. This undesired background signal was not present on control glass surfaces, and must thus be attributed to a surface alteration occurring during the SU-8 processing. Indeed, if an SU-8 film was simply spin-coated then removed again by immersion in the SU-8 developer, a marked increase in contact angle on the glass support was observed, indicating the formation of some form of contaminating residual layer. The contaminating layer could not be removed by thorough washing in fresh developer or other solvents. Although is was removed by oxygen plasma treatment, oxygen plasma also quickly breaks down the surface epoxide groups on SU-8, prohibiting any specific thiol-epoxide chemistry, so this was not a viable alternative. Finally, wet cleaning with NaOH at 50 °C for 1-5 minutes was able to thoroughly clean the glass, presumably due to slight etching of the glass by NaOH. The cleaning procedure usually did not harm microscale or nanoscale SU-8 features, although detachment was occasionally observed, especially at longer incubation times. The signal from the glass surrounding the SU-8 features after cleaning was indistinguishable from clean glass. All fluorescent measurements were performed after implementing the cleaning procedure, indicating that the specific thiol-based chemistry on SU-8 was not substantially influenced.

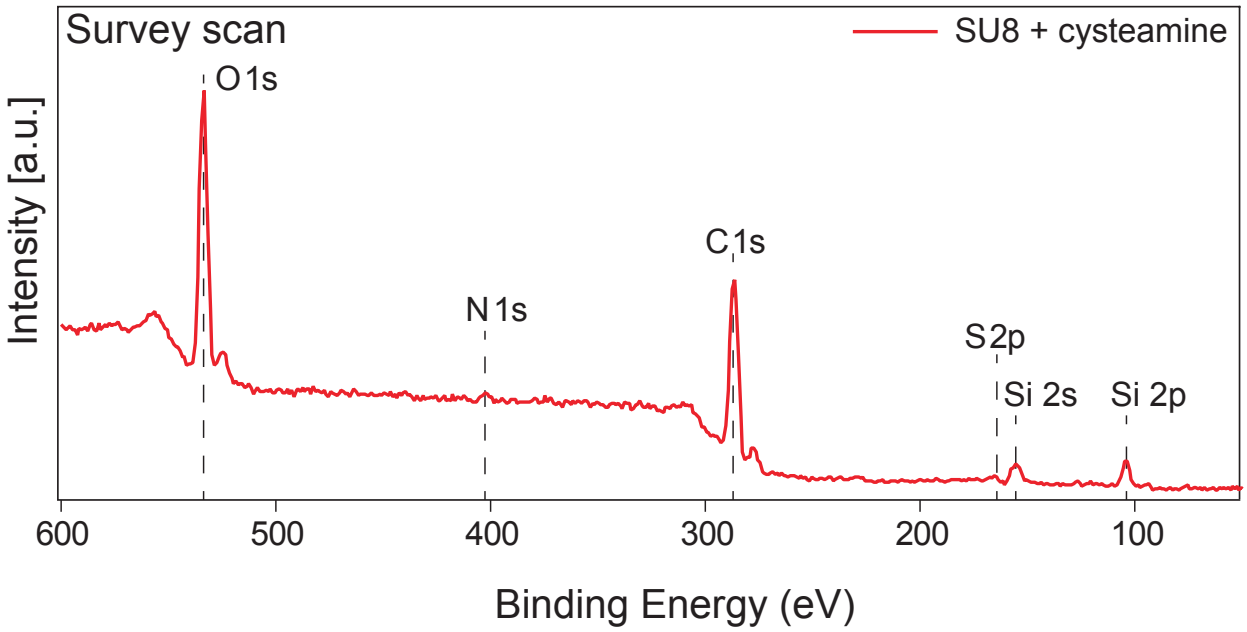

Figure S 5: XPS survey spectra of cysteamine-modified SU-8 film on a silicon wafer (1 hour incubation). The silicon peaks are most likely caused by a signal from the wafer substrate via defects or scratches in the film. Carbon and oxygen peaks originate from both the SU-8 film as well as surface contamination, while the nitrogen and sulphur peaks originate from cysteamine molecules binding to the SU-8.

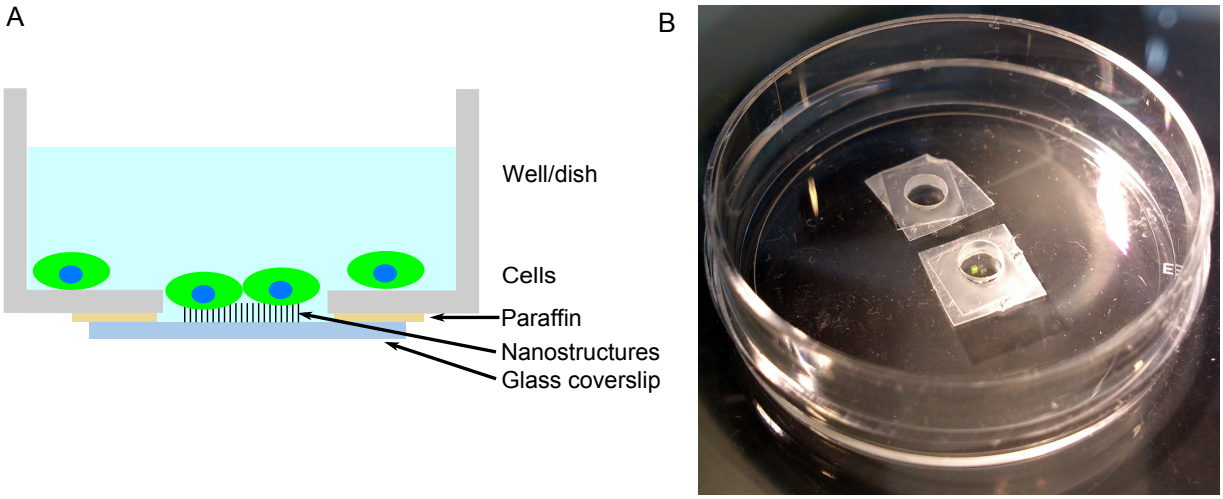

Figure S 6: (A) Schematic view of the mounting of glass coverslips with SU-8 nanostructures into dishes suitable for cell culturing and high resolution live and fixed cell microscopy. Typically, one or more holes of 3.5 mm were drilled into the base of a 35 mm petri dish. A matching hole was punctured in a piece of parafilm. The glass cover slip was then adhered by careful heating on a hot-plate or with a wide-tipped soldering iron until the parafilm melted, creating a water-tight seal. (B) Example of dish used, containing two samples mounted as described in (A).

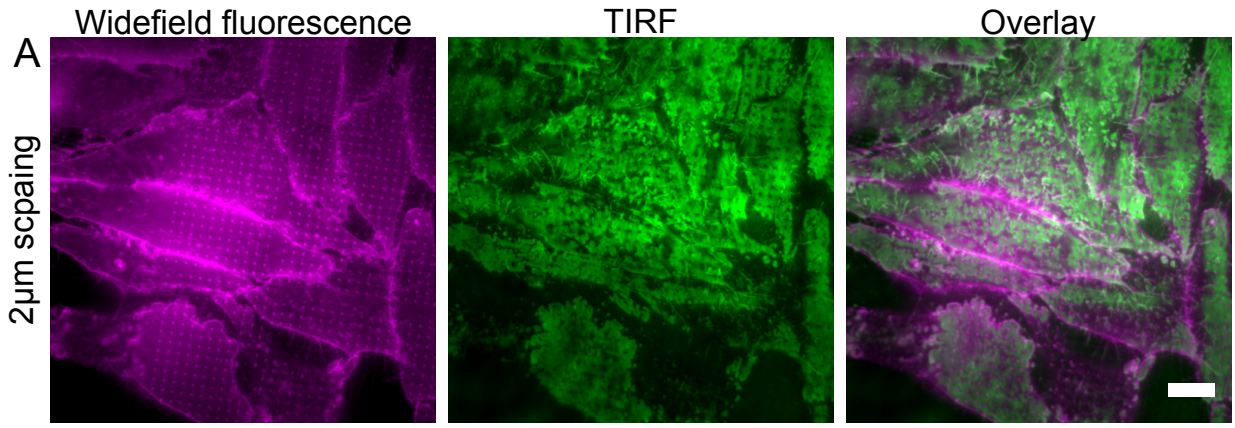

Figure S 7: Widefield and TIRF micrographs of the plasma membrane of CellMask orange-labelled HeLa cells on 1 µm high square nanopillar arrays with 2 µm spacing. An increase of widefield signal could be observed at nanopillar locations (left panel), compared to the membrane on glass (between the nanopillars, and left part of figure with no nanopillars). Corresponding TIRF images (center panel) highlights areas of the cell membrane in contact with the cover slip, demonstrating that the cell membrane is nearly fully in contact with the cover slip at this nanopillar spacing, as opposed to the 1 µm spaced nanopillars described in the main text.

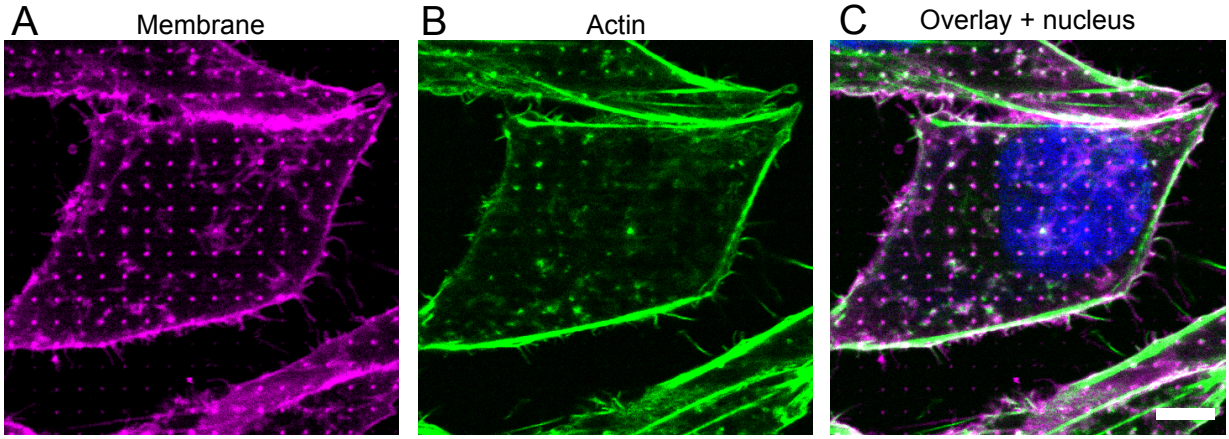

Figure S 8: Scanning confocal micrograph of HeLa cells growing on 2 µm spaced nanopillar array. The cells were labelled with (A) CellMask orange for the plasma membrane (magenta), (B) phalloidin-Alexa488 for actin filaments (green) and (C) overlay image with Hoechst 34580 for the nucleus (nucleus). The cell membrane shows an increased signal at each nanopillar site due to wrapping of the cell membrane around the nanopillars, while the actin shows a certain degree of colocalization at some nanopillar sites. Although the colocalization can be observed, further details are obscured by the resolution limits of the confocal microscope, even if these results were acquired at best possible resolution with a 63X 1.4 oil immersion objective. In the main text results on cell membrane and actin conformation are therefore presented and elaborated using superresolution methods such as TIRF, 3D-SIM and STED. Scale bar 5 µm.